J. Am. Ceram. Soc., 98 [3] 811–818 (2015)
DOI: 10.1111/jace.13363

journal

Phase-Composition-Dependent Piezoelectric and Electromechanical Strain Properties in $(Bi_{1/2}Na_{1/2})TiO_3$–$Ba(Ni_{1/2}Nb_{1/2})O_3$ Lead-Free Ceramics

Feng Li,[‡] Ruzhong Zuo,[‡,†] Donggeng Zheng,[‡] and Longtu Li[§]

[‡]Institute of Electro Ceramics & Devices, School of Materials Science and Engineering, Hefei University of Technology, Hefei 230009, China

[§]State Key Laboratory of New Ceramics and Fine Processing, Department of Materials Science and Engineering, Tsinghua University, Beijing 100084, China

New lead-free perovskite solid solution ceramics of $(1-x)(Bi_{1/2}Na_{1/2})TiO_3$–$xBa(Ni_{1/2}Nb_{1/2})O_3$[$(1-x)$BNT–$x$BNN, x = 0.02–0.06) were prepared and their dielectric, ferroelectric, piezoelectric, and electromechanical properties were investigated as a function of the BNN content. The X-ray diffraction results indicated that the addition of BNN has induced a morphotropic phase transformation from rhombohedral to pseudocubic symmetry approximately at x = 0.045, accompanying an evolution of dielectric relaxor behavior as characterized by enhanced dielectric diffuseness and frequency dispersion. In the proximity of the ferroelectric rhombohedral and pseudocubic phase coexistence zone, the x = 0.045 ceramics exhibited optimal piezoelectric and electromechanical coupling properties of d_{33}~121 pC/N and k_p~0.27 owing to decreased energy barriers for polarization switching. However, further addition of BNN could cause a decrease in freezing temperatures of polar nanoregions till the coexistence of nonergodic and ergodic relaxor phases occurred near room temperature, especially for the x = 0.05 sample which has negligible negative strains and thus show the maximum electrostrain of 0.3% under an external electric field of 7 kV/mm, but almost vanished piezoelectric properties. This was attributed to the fact that the induced long-range ferroelectric order could reversibly switch back to its original ergodic state upon removal of external electric fields.

I. Introduction

Lead zirconate titanate based ceramics have been extensively used for transducers, actuators, and sensors due to their excellent piezoelectric and electromechanical properties in the vicinity of morphotropic phase boundary (MPB).[1,2] However, concerns about lead pollution have in recent years spurred considerable efforts to concentrate on lead-free ceramics in consumer products.[3] $(Bi_{1/2}Na_{1/2})TiO_3$ (BNT) with a rhombohedral symmetry ($R3c$) at room temperature was considered to be a promising lead-free ferroelectric ceramic due to its relatively large remanent polarization (P_r~38 μC/cm^2) and high Curie temperature (T_c~320°C) in lead-free piezoelectric materials.[4–6] Although its bottlenecks such as high conductivity and coercive field have restricted practical applications, these drawbacks can be largely alleviated through various methods such as forming typical MPB with $(Bi_{1/2}K_{1/2})TiO_3$ (BKT), $BaTiO_3$ (BT) *et al.*[7–10]

The concept of the tolerance factor (t), being widely used to predict the stability of perovskite structures and provide an indication of how far the atoms can move from the ideal packing position, was first proposed by Goldschmidt *et al.*[11] It can be expressed as $t = (R_A + R_o)/\sqrt{2}(R_B + R_o)$, where R_A, R_B, and R_O are ionic radii of A , B site, and oxygen. Lee *et al.*[12] established a quantitative relation between the MPB composition and the t values in BNT-based ceramics, and they also demonstrated that the t value of the MPB compositions in BNT-based systems was in the vicinity of 0.990–0.993 and should be independent of the added end-members. After that, Hiruma *et al.*[13,14] first put forward an idea that BNT-based solutions should exhibit two types of MPBs. One was the traditional MPB between the ferroelectric rhombohedral and tetragonal phase (assigned to the MPB I), such as BNT–BT,[7,8] BNT–BKT,[9,10] BNT–PT,[15] and the other was the MPB between the ferroelectric rhombohedral and pseudocubic relaxor phases, such as BNT–$SrTiO_3$[16] and BNT–$KNbO_3$.[17] Due to the fact that the latter was correlated with the polymorphic phase transition, for convenience, this kind of MPB was assigned to the MPB II. What is more, Hiruma *et al.* considered that the end-member with high tolerance factors was the prerequisite to form an MPB II for BNT–ABO_3 solid solutions, in which a large strain could be expected during the transformation from the ferroelectric rhombohedral to relaxor pseudocubic state.[13,14] The BNT–BT–$K_{0.5}Na_{0.5}NbO_3$ (KNN) composition, which was initially planned for the use of the pseudoternary system to couple two MPB compositions BNT–BT and BNT–KNN to maximize the electromechanical properties of the given system, was finally found to own a rapid decrease in piezoelectricity and the appearance of a giant strain.[18–20] Afterward, a few BNT-based compositions with large electrostrains were reported.[21–23]

Barium nickel niobate [$Ba(Ni_{1/2}Nb_{1/2})O_3$, abbreviated as BNN] is a perovskite ferroelectric ceramic, which exhibits a diffuse phase transition and possesses a cubic structure at room temperature.[24] According to Shannon's reports,[25] BNN has a tolerance factor of t = 1.064 (R_{Ba}^{2+} = 1.61 Å, R_{Ni}^{3+} = 0.56 Å, and R_{Nb}^{5+} = 0.64 Å) and seems possible to form MPB II with BNT. In this study, a binary solid solution of BNT–BNN was designed and fabricated. The phase composition dependence of its dielectric, ferroelectric, piezoelectric properties, and electromechanical strain properties was systematically investigated as a function of the BNN content.

II. Experimental Procedures

The $(1-x)$BNT–xBNN (x = 0.02–0.06) piezoelectric ceramics were synthesized by a conventional solid-state reaction method using high-purity chemicals: Bi_2O_3 (99.0%), Na_2CO_3 (99.8%), $BaCO_3$ (99.0%), $C_4H_6NiO_4{\cdot}4H_2O$ (99.0%), Nb_2O_5

D. Viehland—contributing editor

Manuscript No. 35438. Received August 8, 2014; revised October 9, 2014; approved November 5, 2014.
[†]Author to whom correspondence should be addressed. e-mail: rzzuo@hotmail.com

(99.5%), and TiO_2 (99.0%) as raw materials. The powders were weighed and ball-milled with ethanol and zirconia media for 6 h, then the slurry was dried at 100°C. Nickel acetate was used in this study instead of nickel oxide (NiO) to obtain a higher reactive activity, although its reprecipitation problem during drying may induce the powder inhomogeneity. This issue was solved by repeatedly grinding and sieving the powder mixture. Moreover, the powders were calcined twice in a closed alumina crucible at 850°C for 3 h. After calcination, the mixture was ball-milled again for 10 h with 1 wt% PVB as a binder. The granulated powder was uniaxially pressed into disks with a diameter of 10 mm and a thickness of 1 mm. The compacted disks were sintered in the temperature of 1100°C–1160°C for 2 h. To minimize the vaporization of Na and Bi, sample disks were buried in the sacrificial powder of the same composition. For the electrical measurements, silver paste was painted on major sides of the disks and fired at 550°C for 30 min as the electrodes. The specimens were polarized in the silicone oil bath at room temperature under a dc field of 5–7 kV/mm for 15 min.

The phase structures were analyzed at room temperature by an X-ray diffractometer (XRD; D/Mzx-rB, Rigaku, Tokyo, Japan) with Cu$K_{\alpha 1}$ radiation. The dielectric properties were measured at various frequencies using an LCR meter (Agilent E4980A; Santa Clara, CA) in a temperature range 20°C–400°C and in a frequency range 10 kHz–1 MHz. The piezoelectric strain constant d_{33} of poled samples was measured by a Belincourt-meter (YE2703A; Sinocera, Yangzhou, China). The planar electromechanical coupling factor k_p was determined by a resonance–antiresonance method using an impedance analyzer (PV70A; Beijing Band ERA Co. Ltd., Beijing, China). A ferroelectric test system (Precision LC; Radiant Technologies, Inc. Albuquerque, NM) was used to measure the polarization–electric field (P–E) hysteresis loops and electric-field-induced strain (S–E) curves.

III. Results and Discussion

Figure 1(a) shows the XRD patterns of $(1-x)$BNT–xBNN ceramics. It can be seen that all the compositions exhibit a pure perovskite structure and no obvious second phases could be detected. That is to say, Ba^{2+} and $(Ni_{1/2}Nb_{1/2})^{4+}$ ions have completely diffused into the lattice and formed a solid solution with BNT. The asymmetry of (111) diffraction peaks and nonsplitting of the (200) peaks for the x = 0.02–0.04 samples suggest that these compositions may own a rhombohedral structure. When the BNN content was increased up to 0.05, 0.0525, and 0.06, single peaks of (111) and (200) profiles could be clearly seen, which illustrates that these three compositions should display a pseudocubic perovskite structure in combination with the analysis of the macroscopic properties infra. To give an insight into the room-temperature phase structure, the slowly scanned (111) peaks were fitted by using Gaussian peak shape function for samples with x = 0.02–0.05, as shown in Figs. 1(b1)–(b5). The structural symmetry of the samples can be well established from the peak splitting and the relative intensity of these reflection lines. It can be clearly seen that the samples with x = 0.02, 0.03, and 0.04 display a rhombohedral structure due to the splitting of (111) peaks (as denoted by arrows). However, the $(111)_R/(-111)_R$ and $(111)_{PC}$ peaks could be simultaneously detected in the x = 0.045 sample, indicating the coexistence of rhombohedral and pseudocubic phases. The single (111) peak for samples with x = 0.05, 0.0525, and 0.06 indicates a pseudocubic symmetry. For simplicity, only the x = 0.05 sample was used as an example here. It seems also possible to fit the XRD data of the x = 0.045 sample using a single Gaussian peak. However, the best fit was obtained for this sample as the existence of rhombohedral and pseudocubic phases was considered. This is because the goodness of fit (r^2 = 0.998) value extracted by using three Gaussian peaks is bigger than that in the case of a single Gaussian peak (r^2 = 0.984). In a word, the ferroelectric rhombohedral distortion gradually decreased with increasing the BNN content and finally evolved into a pseudocubic structure starting from x = 0.05. Based on the XRD data, the lattice constant a was calculated by fitting the diffraction peak profile with a pseudocubic-Voigt profile function using the program of MDI Jade 6.0, as shown in Fig. 1(c). It can be obviously seen that the lattice constant a increased slightly with increasing the BNN content, suggesting that there is a slight lattice expansion. This is probably due to the relatively large ionic radii of Ba^{2+} compared with Bi^{3+} and Na^{+} at the A sites (CN = 12, $R_{(Bi1/2Na1/2)^{2+}}$ = 1.42 Å < $R_{Ba^{2+}}$ = 1.64 Å), although the B-site average ionic radii of $(Ni_{1/2}Nb_{1/2})^{4+}$ (CN = 6, $R_{(Ni1/2Nb1/2)^{4+}}$ = 0.60 Å) are slightly smaller than that of Ti^{4+} (CN = 6, $R_{Ti^{4+}}$ = 0.605 Å).[25]

Figure 2 shows the SEM micrographs of $(1-x)$BNT–xBNN ceramics with x = 0.02–0.06. It can be noted that the grains of all samples grow extremely well and are closely packed with almost no pores, indicating of high densities. Moreover, with increasing the BNN content, the grain size only slightly increases from ~20.1 μm for the x = 0.02 sample to ~23.2 μm for the x = 0.06 sample as estimated using a linear intercept method. Although the sample microstructure should be closely correlated to the final electrical properties, yet a slight change in this study will not make an obvious difference in the corresponding dielectric and ferroelectric properties. Good densification behavior of the studied lead-free materials would provide an additional advantage as compared to alkaline niobate based lead-free compositions.

Figure 3 shows that temperature and frequency dependences of dielectric permittivity of unpoled and poled $(1-x)$ BNT–xBNN ceramics (x = 0.02–0.06) with changing the measuring frequency from 10 kHz to 1 MHz. It is obvious that all samples show a strong frequency dispersion around the temperature at the dielectric maxima (T_m), which illustrates that these samples can be classified as relaxor ferroelectrics.[26] The evolution of the relaxor behavior was believed to derive from the change in the size and dynamics of the polar nanoregions (PNRs). The PNRs usually appear at a temperature of a few hundred degrees above the Curie temperature and the macroscopic polarization completely disappears in this temperature region,[26–29] during which the PNRs are randomly distributed and exist in an ergodic state. Then, the average size of PNRs increases and their dynamics slow down during cooling. The ergodic PNRs would then either transform into microsized domains at a temperature called as T_{FR} to form normal ferroelectrics or be frozen into a static polar order of nonergodic relaxor state below a critical freezing temperature T_f.[30–32] Generally speaking, PNRs were determined by a local random field owing to the disorder distribution of different ions at one or more equivalent crystallographic sites of the structure. In this system, incorporation of Ba^{2+} ions at the A site and $(Ni_{0.5}Nb_{0.5})^{4+}$ complex ions at the B site led to the increase in the relaxor behavior. For poled ceramics, the dielectric anomaly at lower temperatures T_{FR} could be more clearly seen as x = 0.02–0.045. This anomaly was referred as a transformation from the rhombohedral ferroelectric order to the relaxor state, corresponding to the frequency-independent peaks in the dielectric curves [the inflection point was indicated by arrows in the insets of Figs. 3(a)–(d)]. Moreover, in contrast to nearly invariant T_m values, T_{FR} sharply decreases from 194°C for x = 0.02 to 67°C for x = 0.045, and cannot be detected above room temperature in the dielectric curves as $x \geq 0.05$. Although an obvious anomaly peak was not seen in poled samples with $x \geq 0.05$, yet the value of dielectric permittivity for poled samples was suppressed compared with unpoled samples, as shown in Figs. 3(h), (i) and (j). As known, dielectric permittivity can be influenced by the mobility and density of the domain walls. Higher dielectric permittivity for unpoled relaxor states may be due to the existence of polar nanodomains.[33] As the electric field is applied, the long-range ferroelectric order is established and large domains appear, then

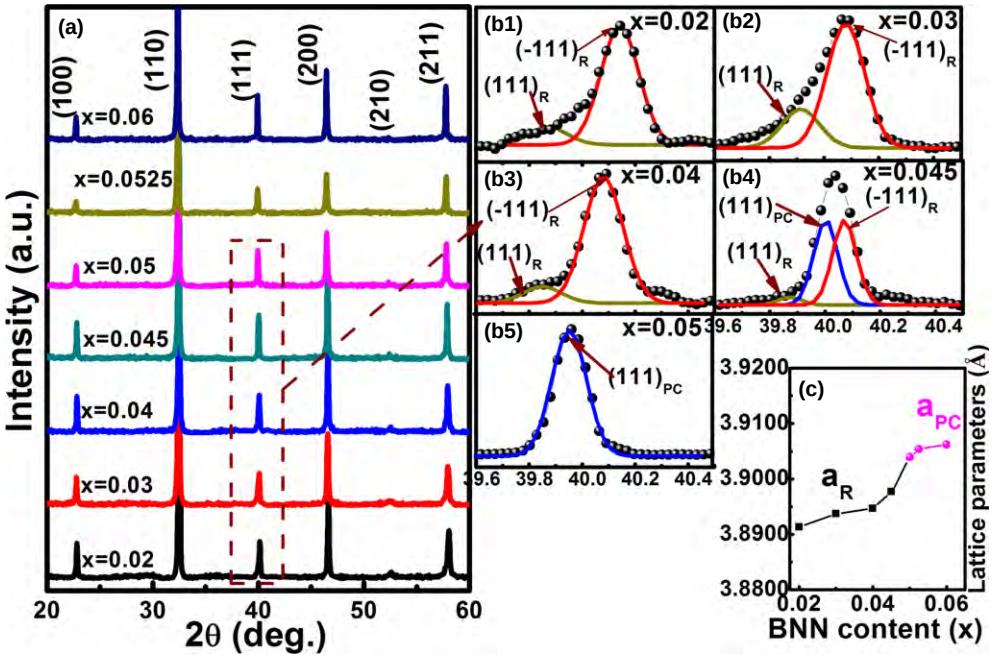

Fig. 1. (a) Room-temperature XRD patterns of $(1-x)$BNT–xBNN ceramics (x = 0.02–0.06), (b1)~(b5) the (111) diffraction peaks fitted by using PeakFit software with the Gaussian profile for the x = 0.02–0.05 samples, and (c) the variation in the lattice parameter a with respect to the BNN content.

resulting in a degradation of dielectric permittivity. For samples with x = 0.0525 and 0.06, no obvious difference can be detected in the dielectric curves before and after poling, indicating that these two samples are completely of ergodic sates above room temperature. For the same reason, the x = 0.05 sample should possibly lie in the coexistence zone of ergodic and nonergodic relaxor phases at room temperature but should be dominated by ergodic relaxor phases.

Figure 4(a) shows the inverse dielectric permittivity versus temperature curves for $(1-x)$BNT–xBNN ceramics as indicated. For a normal ferroelectric, it is known that the dielectric permittivity above its Curie temperature follows the Curie–Weiss law: $1/\varepsilon = (T-T_c)/C$,[34] where T_c is the Curie temperature and C is the Curie–Weiss constant. Nevertheless, it is found that the inverse dielectric permittivity of $(1-x)$ BNT–xBNN ceramics (x = 0.02, 0.04, and 0.06) shows an obvious deviation from the Curie–Weiss law, which can be denoted as ΔT_m given by the following equation: $\Delta T_m = T_{cw}-T_m$, where T_{cw} denotes the temperature where the inverse dielectric permittivity begins to deviate from the Curie–Weiss law. This deviation was commonly observed in relaxor ferroelectrics.[26] As a matter of fact, for relaxor ferroelectrics, the diffuseness of phase transition can be accounted for more effectively by a modified Curie–Weiss law $1/\varepsilon - 1/\varepsilon_m = C^{-1}(T-T_m)^{\gamma}$,[35] where γ denotes the degree of diffuseness, and ε_m stands for the maximum dielectric permittivity at a fixed frequency. Generally speaking, the parameter γ ranges from one for a normal ferroelectric to two for an ideal relaxor ferroelectric. The plots of $\ln(1/\varepsilon-1/\varepsilon_m)$ versus $\ln(T-T_m)$ for three compositions (x = 0.02, 0.04, and 0.06) exhibit a well linear relationship, as shown in Fig. 4(b). The γ values for different compositions can be obtained from the slope of the fitted lines. In addition, the parameter ΔT_{relax}, which is defined as the difference between two T_m values at 1 MHz and 10 kHz, was introduced to investigate the relaxation degree of ferroelectric ceramics. As can be seen from Fig. 4(c), three of ΔT_{relax} and γ and increase with increasing the BNN content, indicating that the relaxor behavior of the system was obviously enhanced with increasing the BNN content. Such a phenomenon can also be seen in other lead-free piezoelectric ceramics.[36,37]

Figures 5(a)–(g) show the composition dependence of the room-temperature P–E loops for samples with x = 0.02–0.06, together with the corresponding current density loops (J–E). It is obvious that saturated and square P–E loops combined with one single-sharp current density peak P1 appear in samples with x = 0.02–0.04, which can be ascribed to the domain switching of long-range ferroelectric order ($x \le 0.04$) or short-range polar order (nonergodic phases) (x = 0.045, 0.05). When the BNN content reached 0.045 and 0.05, slightly pinched P–E loops with an additional current density peak P2 can be clearly observed, probably due to the coexistence of ergodic and nonergodic relaxor phase.[38–41] The induced long-range ferroelectric order would revert back to its initial ergodic state as the applied electric field was released, generating the second polarization current peak P2. By comparison, very slim P–E loops in the absence of obvious polarization current peaks were observed in samples with $x \ge 0.0525$, indicating that the samples should exhibit a pure ergodic state at room temperature. The above statements are also in good agreement with the dielectric measurements. The variation tendency of the maximum polarization (P_{max}), remanent polarization (P_r), and coercive field (E_c) values with changing the BNN content is shown in Fig. 5(h). Compared with the change in P_r, the P_{max} value does not change much for different compositions because the latter is mainly related to the poling state of the (electric field induced) long-range ferroelectric states, although both of them seem to have the maximum values at x = 0.045. This may be due to the easier domain switching under an external electric field near the ferroelectric phase coexistence zone through the addition of BNN into BNT. It can be seen that the P_r value reaches the minimum as $x > 0.05$. Although a long-range ferroelectric state can be induced from an ergodic state by an electric field, yet it becomes more unstable as the relaxor degree of the sample increases due to an increase in the local random field. The P_r value for the $0.045 \le x \le 0.05$ samples is relatively large compared to the $x > 0.05$ sample because of a small amount of ferroelectric order irreversibly transformed from nonergodic phases.[32] As expected, the E_c value approximately defined as the electric field when the P_r becomes zero drops monotonously with increasing the BNN content, which can be ascribed to the increased domain switching dynamics because of the disruption of long-range ferroelectric order.

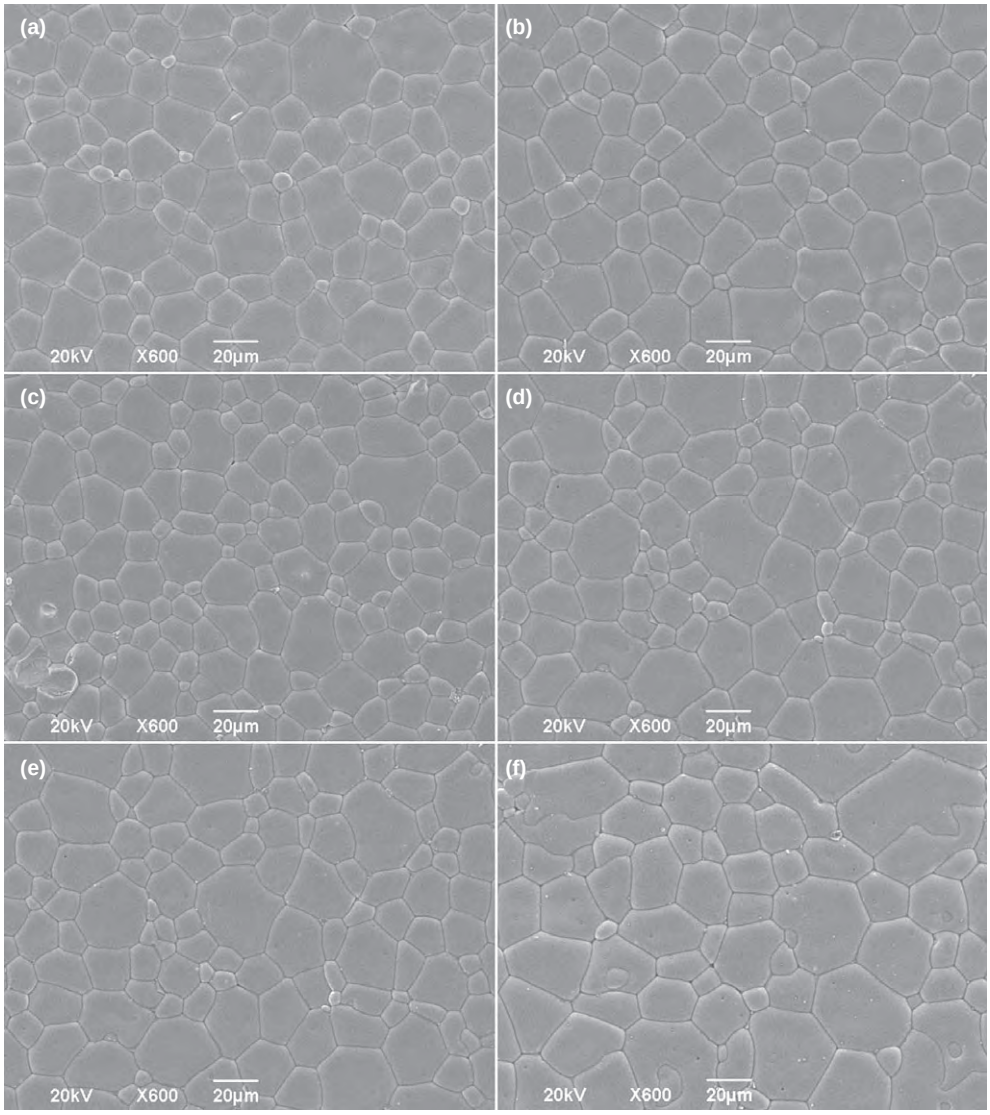

Fig. 2. Typical SEM micrographs of $(1-x)$BNT–xBNN ceramics sintered at their optimal temperatures: (a) $x = 0.02$, (b) $x = 0.03$, (c) $x = 0.045$, (d) $x = 0.05$, (e) $x = 0.0525$, and (f) $x = 0.06$.

Figure 6 shows that the bipolar and unipolar strain loops measured at room temperature under an electric field of 7 kV/mm. For bipolar S–E curves, $(1-x)$BNT–x BNN ($x \leq 0.045$) samples generally exhibit a butterfly strain loop with a large negative strain S_{neg}, which is typical for ferroelectrics. With the further incorporation of BNN ($x \geq 0.05$), the butterfly like loop drastically changes into the sprout-shaped loop, accompanied by a drastic decrease in the negative strain S_{neg} and a concurrent increase in the positive strain S_{pos}, as shown in Fig. 6(a). Figure 6(b) shows that the unipolar strain curves change with respect to the BNN content. The maximum unipolar strain of 0.3% appears in the sample with $x = 0.05$. The definition of S_{pos} and S_{neg} was explained in Fig. 6(c). Both of them change as a function of the BNN content, as shown in Fig. 6(d). It is obvious that the absolute value of S_{neg} first increase until the BNN content is up to 0.045. The increment of the absolute value of S_{neg} may also originate from the easier domain switching near the phase coexistence zone, which is in agreement with the variation in P_r [Fig. 5(h)]. When the BNN content rises to 0.05, the appearance of dominant ergodic phases may be responsible for the sharp decrease in S_{neg}, which also keeps a good agreement with the variation in P_r. Interestingly, it can be seen that S_{pos} steadily increases and reaches its maximum value of ~0.3% in the vicinity of $x = 0.05$, as shown in Fig. 6(d). An obvious increase in the electric field induced strains was usually correlated with the coexistence of ergodic and nonergodic phases, in which ergodic phases can be reversibly and easily transformed into a long-range ferroelectric order under an external electric field.[20,42] Further addition of BNN tends to decrease the S_{pos} value because the phase composition in the sample has been away from the phase coexistence zone so that the transformation from an ergodic phase to a ferroelectric phase becomes rather hard. Similar phenomena have also been observed in other Bi-containing perovskite-structured ferroelectrics.[38–43]

Figure 7(a) shows that the small-signal d_{33}, k_p and large-signal piezoelectric constant d_{33}* (also defined as the normalized strain S_{max}/E_{max}) as a function of the BNN content. With increasing the BNN content, both d_{33} and k_p first increase gradually and reach the maximum value of 121 pC/N and 0.27, respectively, at $x = 0.045$, which should be ascribed to relatively low-energy barrier for polarization switching provided by coexisting ferroelectric rhombohedral and pseudocubic phases.[44] Moreover, the formation of nanodomains may also help to reduce the domain wall energy owing to the existence of pseudocubic nonergodic relaxor phases.[45] However, with a further introduction of BNN, the d_{33} and k_p values drastically decrease and nearly approach to zero at $x = 0.05$–0.06 owing to the completely reversible phase transition to ergodic phases. It is worthy of note that the nonzero d_{33} value for the $x = 0.05$ sample may demonstrate that a little trace of nonergodic relaxor phase still exists in this composition range. At the moment when the d_{33} and

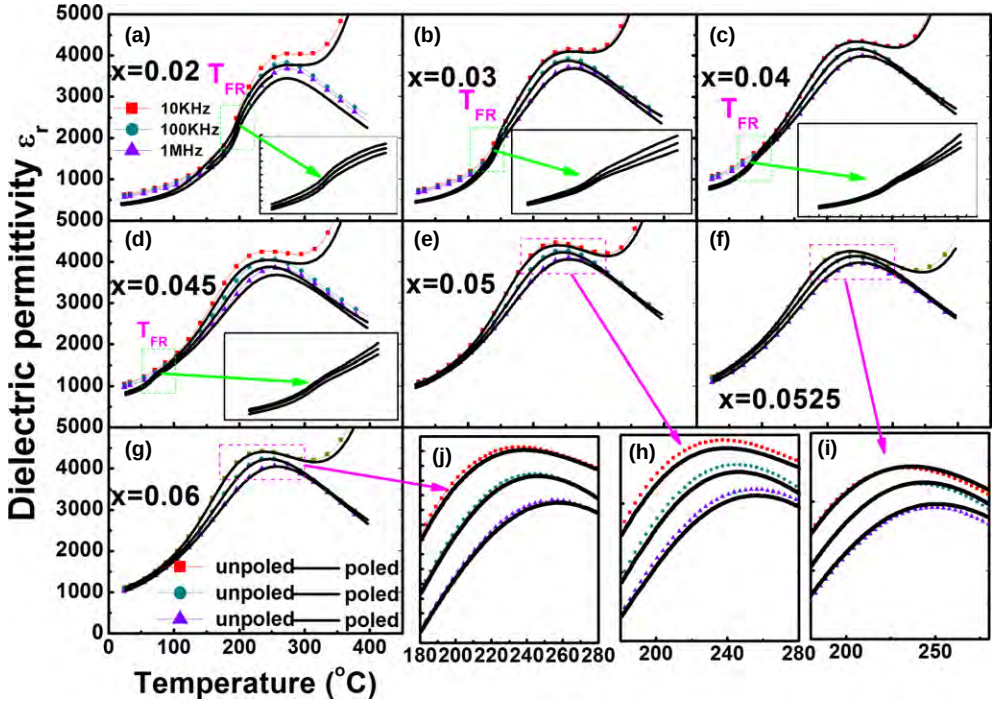

Fig. 3. Dielectric permittivity of unpoled and poled $(1-x)$BNT–xBNN ceramics as a function of temperature and frequency for samples with (a) $x = 0.02$, (b) $x = 0.03$, (c) $x = 0.04$, (d) $x = 0.045$, (e) $x = 0.05$, (f) $x = 0.0525$, and (g) $x = 0.06$; (h), (i) and (j) the locally magnified curves in fig. 3(e), (f), and (g) in the temperature range 180°C–280°C, respectively.

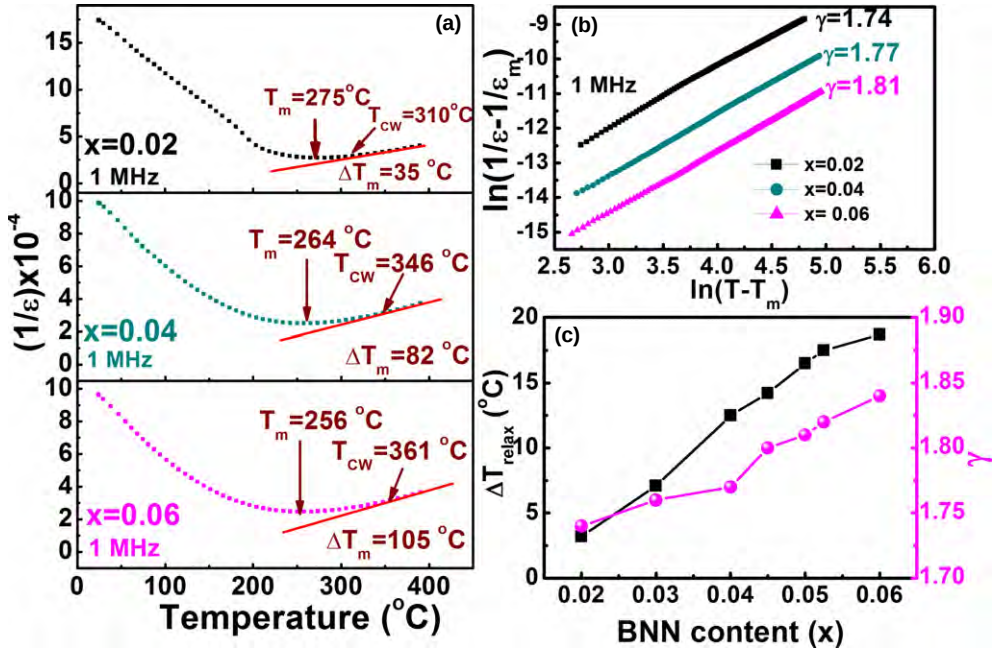

Fig. 4. (a) Inverse dielectric permittivity versus temperature curves for samples as indicated, (b) the $\ln(1/\varepsilon - 1/\varepsilon_m)$ versus $\ln(T - T_m)$ curves at 1 MHz for samples as indicated, and (c) the variation in both ΔT_{relax} and γ as a function of the BNN content.

k_p values significantly decrease, the d_{33}* value sharply increases to a maximum value of ~420 pm/V in the composition with $x = 0.5$, being derived from a crossover from a dominant nonergodic phase to a dominant ergodic relaxor phase. It can be seen that the quasistatic piezoelectric properties and dynamic large-signal strain properties are dominated by the contribution from the irreversible domain switching (i.e., the maximum P_r) and the recoverable ergodic–ferroelectric phase transformation (i.e., near-zero S_r), respectively. Moreover, the values of piezoelectric and ferroelectric properties are notably higher than those of $Bi_{0.5}Na_{0.5}TiO_3$–$BiCoO_3$ (BNT–BC), BNT–$Bi(Mg_{0.5}Ti_{0.5})TiO_3$ (BNT–BMT), $Bi_{0.5}Na_{0.5}TiO_3$–$Bi(Al_{0.5}Ga_{0.5})O_3$ (BNT–BAG) compositions, *et al.*,[46–50] and are comparable with those of $Bi_{0.5}Na_{0.5}TiO_3$–$Ba(Al_{0.5}Ta_{0.5})O_3$ (BNT–BAT) and $Bi_{0.5}Na_{0.5}TiO_3$–$SrTiO_3$ (BNT–ST) systems.[16,51] The comparison of the piezoelectric and ferroelectric properties among those BNT-based binary solid solution ceramics was made, as shown in Table I. Combined with the XRD data, dielectric, ferroelectric, and piezoelectric properties analyzed above, a schematic phase diagram was constructed, indicating different phase regions with changing the BNN content and temperature, as shown in Fig. 7(b). The characteristic temperatures such as T_{cw}, T_{FR}, and T_m have been discussed

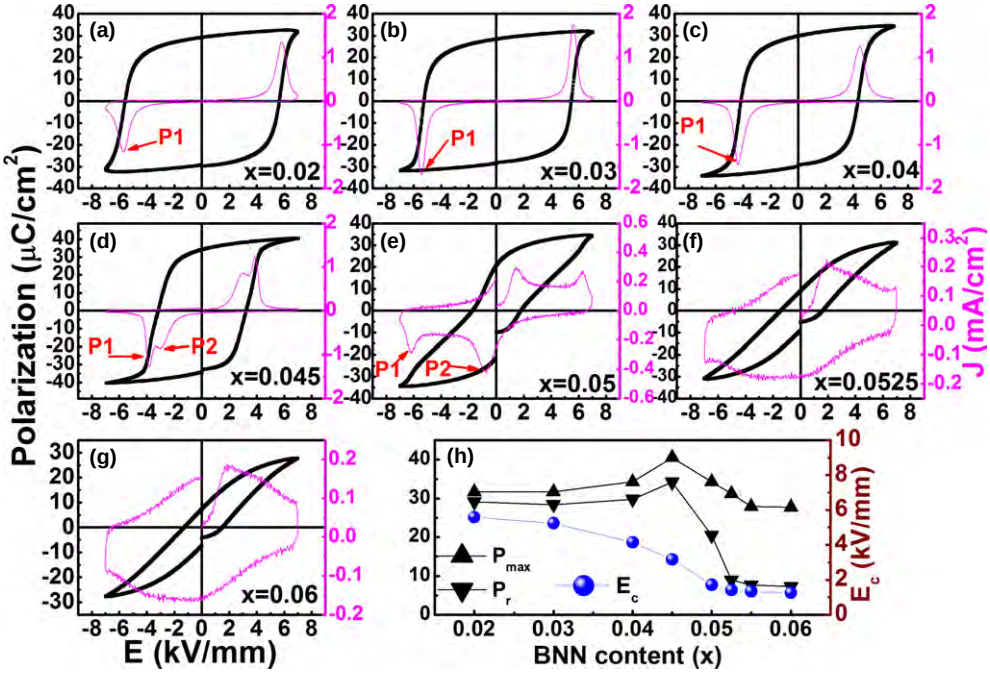

Fig. 5. *P–E* hysteresis loops together with *J–E* curves measured at a frequency of 1 Hz for $(1-x)$BNT-xBNN ceramics: (a) $x = 0.02$, (b) $x = 0.03$, (c) $x = 0.04$, (d) $x = 0.045$, (e) $x = 0.05$, (f) $x = 0.0525$, and (g) $x = 0.06$; (h) the variation in the maximum polarization P_{max}, remanent polarization P_r and the zcoercive field E_c values against the BNN content.

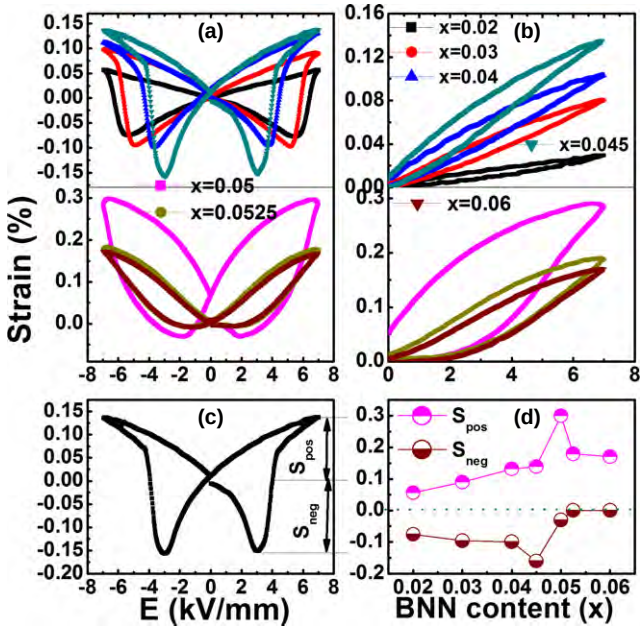

Fig. 6. (a) Bipolar and (b) unipolar *S–E* curves for samples as indicated, (c) the indication of both S_{pos} and S_{neg} values, and (d) S_{pos} and S_{neg} values at room temperature as a function of the BNN content.

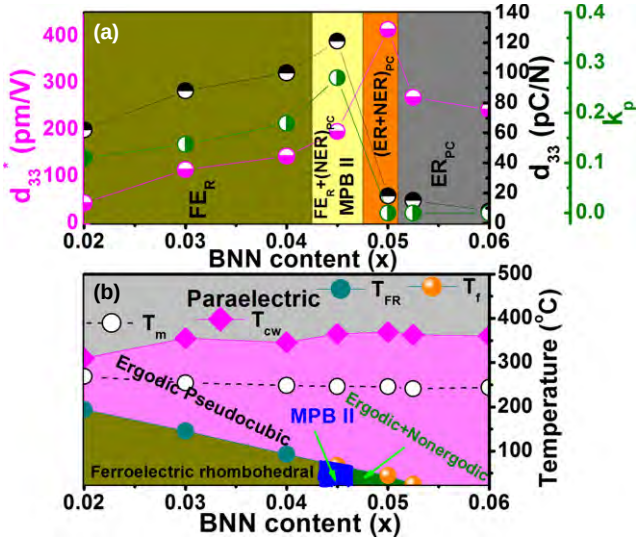

Fig. 7. (a) Piezoelectric strain coefficient d_{33}, electromechanical coupling coefficient k_p and normalized strain d_{33}^* of $(1-x)$BNT–xBNN ($x = 0.02$–0.06) ceramics as a function of the BNN content, and (b) the schematic phase diagram of $(1-x)$BNT–xBNN ceramics.

supra. The freezing temperature T_f should have been obtained by fitting the measured dielectric permittivity versus temperature curves at different frequencies for unpoled

Table I. Piezoelectric and Ferroelectric Properties of BNT-Based Binary Solid Solution Ceramics

	d_{33} (pC/N)	k_p	Strain (%)	d_{33}* (pm/V)	P_{max} (μC/cm²)	P_r (μC/cm²)	E_c (kV/mm)	References
BNT–BC	107	~0.13	~0.12	~150	~40	~35	~5	46
BNT–KNN	94	~0.25	~0.22	~275	~30	~20	~1.5	47
BNT–BAG	93	/	~0.09	~100	~30	~25	~5	48
BNT–BZT	92	~0.22	~0.15	~188	~28	~18	~2.5	49
BNT–BMT	110	/	~0.12	~150	~38	~25	~3	50
BNT–BAT	127	/	~0.36	~448	~37	~17	~2	51
BNT–ST	127	/	~0.29	~488	~35	~10	~2	16
BNT–BNN	121	~0.27	~0.3	~420	~34	~20	~1.7	This study

samples (Fig. 3) to the Vogel–Fulcher relationship.[28] It was shown that piezoelectric and electromechanical strain properties exhibit an obvious phase compositional dependence. Near the transition zone (MPB II) between the ferroelectric rhombohedral and pseudocubic relaxor phase, the optimal piezoelectric and electromechanical coupling properties were obtained in the vicinity of $x = 0.045$. By comparison, the coexistence of ergodic and nonergodic relaxor phases in an appropriate amount mainly contributes to the appearance of significantly enhanced eletrostrains around the $x = 0.05$ composition. The basic reasons for the phase-composition-dependent piezoelectric and strain properties are based on the lower energy barrier for the polarization switching (or domain wall motion) and phase transition provided by coexisting two phases in an appropriate ratio.

IV. Conclusions

$(1-x)$BNT–xBNN binary solid solution ceramics were fabricated via a solid-state reaction method and their dielectric, ferroelectric, piezoelectric, and electromechanical strain properties were systematically investigated as a function of the BNN content, showing a strong phase composition dependence. For the composition with $x = 0.045$, the optimal d_{33} (~121 pC/N) and k_p value (~0.27) were obtained, which are also relatively high as compared to the pure BNT ceramic and other BNT-based binary compositions. Moreover, further addition of BNN would induce an obviously enhanced electrostrain (d_{33}^*~420 pm/V) in the vicinity of $x = 0.05$ because of the coexistence of nonergodic and ergodic phases, but simultaneously lead to completely vanished piezoelectric properties.

Acknowledgments

Financial support from the National Natural Science Foundation of China (grant no. 51472069, U1432113, 51332002) and an opening fund of State Key Laboratory of New Ceramic and Fine Processing at Tsinghua University is gratefully acknowledged.

References

[1]B. Jaffe, W. R. Cook, and H. Jaffe, *Piezoelectric Ceramics*. Academic Press, New York, 1971.

[2]G. H. Haertling, "Ferroelectric Ceramics: History and Technology," *J. Am. Ceram. Soc.*, **82** [4] 797–818 (1999).

[3]J. Rödel, W. Jo, K. T. P. Seifert, E. M. Anton, T. Granzow, and D. Damjanovic, "Perspective on the Development of Lead-Free Piezoceramics," *J. Am. Ceram. Soc.*, **92** [6] 1153–77 (2009).

[4]G. A. Smolenskii, V. A. Isupov, A. I. Agranovskaya, and N. N. Krainik, "New Ferroelectrics of Complex Composition IV," *Sov. Phys. Solid State (Engl. Transl.)*, **2** [11] 2651–4 (1961).

[5]C. F. Buhrer, "Some Properties of Bismuth Perovskites," *J. Chem. Phys.*, **36**, 798–803 (1962).

[6]J. Suchanicz, K. Roleder, A. Kania, and J. Handerek, "Electrostrictive Strain and Pyroeffect in the Region of Phase Coexistence in $Na_{0.5}Bi_{0.5}TiO_3$," *Ferroelectrics*, **77**, 107–10 (1988).

[7]T. Takenaka, K. Maruyama, and K. Sakata, "$(Bi_{1/2}Na_{1/2})TiO_3$-$BaTiO_3$ System for Lead Free Piezoelectric Ceramics," *Jpn. J. Appl. Phys.*, **30**, 2236–9 (1991).

[8]S. T. Zhang, A. B. Kounga, E. Aulbach, and Y. Deng, "Temperature-Dependent Electrical Properties of $0.94Bi_{0.5}Na_{0.5}TiO_3$–$0.06BaTiO_3$ Ceramics," *J. Am. Ceram. Soc.*, **91** [12] 3950–4 (2008).

[9]K. Yoshii, Y. Hiruma, H. Nagata, and T. Takenaka, "Electrical Properties and Depolarization Temperature of $(Bi_{1/2}Na_{1/2})TiO_3$-$(Bi_{1/2}K_{1/2})TiO_3$ Lead-Free Piezo- Electric Ceramics," *Jpn. J. Appl. Phys.*, **45** [5B] 4493–6 (2006).

[10]A. Sasaki, T. Chiba, Y. Mamiya, and E. Otsuki, "Dielectric and Piezoelectric Properties of $(Bi_{0.5}Na_{0.5})TiO_3$-$(Bi_{0.5}K_{0.5})TiO_3$ System," *Jpn. J. Appl. Phys.*, **38**, 5564–7 (1999).

[11]O. Muller and R. Roy, *The Major Ternary Structural Families*, p. 221. Springer,New York, NY, 1974.

[12]W. C. Lee, C. Y. Huang, L. K. Tsao, and Y. C. Wu, "Chemical Composition and Tolerance Factor at the Morphotropic Phase Boundary in $(Bi_{0.5}Na_{0.5})TiO_3$-Based Piezoelectric Ceramics," *J. Eur. Ceram. Soc.*, **29** [8] 1443–8 (2009).

[13]Y. Hiruma, H. Nagata, and T. Takenaka, "Formation of Morphotropic Phase Boundary and Electrical Properties of $(Bi_{1/2}Na_{1/2})TiO_3$-$Ba(Al_{1/2}Nb_{1/2})O_3$ Solid Solution Ceramics," *Jpn. J. Appl. Phys.*, **48**, 09KC08, 6pp (2009).

[14]Y. Hiruma, H. Nagata, and T. Takenaka, "Detection of Morphotropic Phase Boundary of $(Bi_{1/2}Na_{1/2})TiO_3$-$Ba(Al_{1/2}Sb_{1/2})O_3$ Solid Solution Ceramics," *Appl. Phys. Lett.*, **95**, 052903, 3pp (2009).

[15]K. Sakata, T. Takenaka, and Y. Naitou, "Phase Relations, Dielectric and Piezoelectric Properties of Ceramics in the System $(Bi_{0.5}Na_{0.5})TiO_3$-$PbTiO_3$," *Ferroelectrics*, **131**, 219–26 (1992).

[16]Y. Hiruma, Y. Imai, Y. Watanabe, H. Nagata, and T. Takenaka, "Large Electrostrain Near the Phase Transition Temperature of $(Bi_{0.5}Na_{0.5})TiO_3$-$SrTiO_3$ Ferroelectric Ceramics," *Appl. Phys. Lett.*, **92**, 262904, 3pp (2008).

[17]G. F. Fan, W. Z. Lu, X. H. Wang, F. Liang, and J. Z. Xiao, "Phase Transition Behaviour and Electromechanical Properties of $(Na_{1/2}Bi_{1/2})TiO_3$-$KNbO_3$ Lead-Free Piezoelectric Ceramics," *J. Phys. D: Appl. Phys.*, **41**, 035403, 6pp (2008).

[18]W. Jo, R. Dittmer, M. Acosta, J. D. Zang, C. Groh, E. Sapper, K. Wang, and J. Rödel, "Giant Electric-Field-Induced Strains in Lead-Free Ceramics for Actuator Applications–Status and Perspective," *J. Electroceram.*, **29**, 71–93 (2012).

[19]S. T. Zhang, A. B. Kounga, E. Aulbach, H. Ehrenberg, and J. Rödel, "Giant Strain in Lead-Free Piezoceramics $Bi_{0.5}Na_{0.5}TiO_3$-$BaTiO_3$-$K_{0.5}Na_{0.5}NbO_3$ System," *Appl. Phys. Lett.*, **91** [11] 112906, 3pp (2007).

[20]W. Jo, T. Granzow, E. Aulbach, J. Rödel, and D. Damjanovic, "Origin of the Large Strain Response in $K_{0.5}Na_{0.5}NbO_3$-Modified $Bi_{0.5}Na_{0.5}TiO_3$-$BaTiO_3$ Lead-Free Piezoceramics," *J. Appl. Phys.*, **105** [9] 094102, 5pp (2009).

[21]J. G. Hao, B. Shen, J. W. Zhai, and H. Chen, "Effect of $BiMeO_3$ on the Phase Structure, Ferroelectric Stability, and Properties of Lead-Free $Bi_{0.5}(Na_{0.80}K_{0.20})_{0.5}TiO_3$ Ceramics," *J. Am. Ceram. Soc.*, **97**, 1776–84 (2014).

[22]J. G. Hao, B. Shen, J. W. Zhai, C. Z. Liu, X. L. Li, and X. Y. Gao, "Switching of Morphotropic Phase Boundary and Large Strain Response in Lead-Free Ternary $(Bi_{0.5}Na_{0.5})TiO_3$-$(K_{0.5}Bi_{0.5})TiO_3$-$(K_{0.5}Na_{0.5})NbO_3$ System," *J. Appl. Phys.*, **113**, 114106, 13pp (2013).

[23]K. Wang, A. Hussain, W. Jo, and J. Rödel, "Temperature-Dependent Properties of $(Bi_{1/2}Na_{1/2})TiO_3$-$(Bi_{1/2}K_{1/2})TiO_3$-$SrTiO_3$ Lead-Free Piezoceramics," *J. Am. Ceram. Soc.*, **95** [7] 2241–7 (2012).

[24]L. J. Raibagkar and S. B. Bajaj, "Poling Effect on the Dielectric, Pyroelectric and Electrical Conductivity of Ferroelectric Ordered-Disordered Ba $(Ni_{0.5}Nb_{0.5})O_3$," *Solid State Ionics*, **108**, 105–8 (1998).

[25]R. D. Shannon, "Revised Effective Ionic Radii and Systematic Studies of Interatomic Distances in Halides and Chalcogenides," *Acta Crystallogr.*, **32**, 751–67 (1976).

[26]L. E. Cross, "Relaxor Ferroelectrics: An Overview," *Ferroelectrics*, **151**, 305–20 (1994).

[27]N. Novak, R. Pirc, M. Wencka, and Z. Kutnjak, "High-Resolution Calorimetric Study of $Pb(Mg_{1/3}Nb_{2/3})O_3$ Single Crystal," *Phys. Rev. Lett.*, **109**, 037601, 5pp (2012).

[28]D. Viehland, S. J. Jang, L. E. Cross, and M. Wuttig, "Freezing of the Polarization Fluctuations in Lead Magnesium Niobate Relaxors," *J. Appl. Phys.*, **68**, 2916–21 (1990).

[29]G. Burns and F. H. Dacol, "Crystalline Ferroelectrics with Glassy Polarization Behavior," *Phys. Rev. B*, **28**, 2527–30 (1983).

[30]G. A. Samara, "The Relaxational Properties of Compositionally Disordered ABO_3 Perovskites," *J. Phys.: Condens. Matter*, **15**, R367–411 (2003).

[31]X. H. Dai, A. DiGiovanni, and D. Viehland, "Dielectric Properties of Tetragonal Lanthanum Modified Lead Zirconate Titanate Ceramics," *J. Appl. Phys.*, **74**, 3399–405 (1993).

[32]A. A. Bokov and Z. G. Ye, "Recent Progress in Relaxor Ferroelectrics with Perovskite Structure," *J. Mater. Sci.*, **41**, 31–52 (2006).

[33]G. Arlt, "Switching and Dielectric Nonlinearity of Ferroelectric Ceramics," *Ferroelectrics*, **189**, 91–101 (1996).

[34]X. G. Tang, X. X. Wang, K. Chew, and H. L. W. Chan, "Relaxor Behavior of (Ba, Sr)$(Zr,Ti)O_3$ Ferroelectric Ceramics," *Solid State Commun.*, **136**, 89–93 (2005).

[35]K. Uchino and S. Nomura, "Critical Exponents of the Dielectric Constants in Diffused-Phase-Transition Crystals," *Ferroelectrics*, **44**, 55–61 (1982).

[36]C. C. Jin, F. F. Wang, L. L. Wei, J. Tang, Y. Li, Q. R. Yao, C. Y. Tian, and W. Z. Shi, "Influence of B-Site Complex-Ion Substitution on the Structure and Electrical Properties in $Bi_{0.5}Na_{0.5}TiO_3$-Based Lead-Free Solid Solutions," *J. Alloy. Compd.*, **585**, 185–91 (2014).

[37]H. C. Yu and Z. G. Ye, "Dielectric Properties and Relaxor Behavior of a New $(1-x)BaTiO_3$–$X BiAlO_3$ Solid Solution," *J. Appl. Phys.*, **103**, 034114, 5pp (2008).

[38]W. L. Zhao, R. Z. Zuo, D. G. Zheng, and L. T. Li, "Dielectric Relaxor Evolution and Frequency-Insensitive Giant Strains in $(Bi_{0.5}Na_{0.5})TiO_3$-Modified $Bi(Mg_{0.5}Ti_{0.5})O_3$-$PbTiO_3$ Ferroelectric Ceramics," *J. Am. Ceram. Soc.*, **97** [6] 1855–60 (2014).

[39]W. L. Zhao, R. Z. Zuo, F. Li, and L. T. Li, "Structural, Dielectric, Ferroelectric and Strain Properties in $CaZrO_3$-Modified $Bi(Mg_{0.5}Ti_{0.5})O_3$-$PbTiO_3$ Solid Solutions," *J. Alloy. Compd.*, **591**, 218–23 (2014).

[40]W. L. Zhao, R. Z. Zuo, J. Fu, and M. Shi, "Large Strains Accompanying Field-Induced Ergodic Phase-Polar Ordered Phase Transformations in $Bi(Mg_{0.5}Ti_{0.5})O_3$-$PbTiO_3$-$(Bi_{0.5}Na_{0.5})TiO_3$ Ternary System," *J. Eur. Ceram. Soc.*, **34**, 2299–309 (2014).

[41]G. Viola, H. Ning, X. J. Wei, M. Deluca, and A. Adomkevicius, "Dielectric Relaxation, Lattice Dynamics and Polarization Mechanisms in $Bi_{0.5}Na_{0.5}$-TiO_3-Based Lead–Free Ceramics," *J. Appl. Phys.*, **114**, 014107, 9pp (2013).

[42]J. Fu and R. Z. Zuo, "Giant Electrostrains Accompanying the Evolution of a Relaxor Behavior in $Bi(Mg_{0.5}Ti_{0.5})O_3$-$PbZrO_3$-$PbTiO_3$ Ferroelectric Ceramics," *Acta Mater.*, **61**, 3687–91 (2013).

[43]J. G. Hao, W. F. Bai, W. Li, B. Shen, and J. W. Zhai, "Phase Transition, Relaxor Behavior, and Large Strain Response in $LiNbO_3$-Modified $Bi_{0.5}(Na_{0.80}K_{0.20})_{0.5}TiO_3$ Lead-Free Piezoceramics," *J. Appl. Phys.*, **114**, 044103, 12pp (2013).

[44]X. M. Liu, H. Z. Guo, and X. L. Tan, "Evolution of Structure and Electrical Properties with Lanthanum Content in $[(Bi_{1/2}Na_{1/2})_{0.95}Ba_{0.05}]_{1-x}La_xTiO_3$ Ceramics," *J. Eur. Ceram. Soc.*, **34**, 2997–3006 (2014).

[45]J. Fu, R. Z. Zuo, and Z. K. Xu, "High Piezoelectric Activity in (Na,K) NbO_3 Based Lead-Free Piezoelectric Ceramics: Contribution of Nanodomains," *Appl. Phys. Lett.*, **99**, 062901, 3pp (2011).

[46]F. F. Guo, B. Yang, S. T. Zhang, X. Liu, L. M. Zheng, Z. Wang, F. M. Wu, D. L. Wang, and W. W. Cao, "Morphotropic Phase Boundary and Electric Properties in $(1-x)Bi_{0.5}Na_{0.5}TiO_3$-$XBiCoO_3$ Lead-Free Piezoelectric Ceramics," *J. Appl. Phys.*, **111**, 124113, 5pp (2012).

[47]A. B. Kounga, S. T. Zhang, W. Jo, T. Granzow, and J. Rödel, "Morphotropic Phase Boundary in $(1-x)Bi_{0.5}Na_{0.5}TiO_3$-$xK_{0.5}Na_{0.5}NbO_3$ Lead-Free Piezoceramics," *Appl. Phys. Lett.*, **92**, 222902, 3pp (2008).

[48]Q. Wang, J. Chen, L. L. Fan, H. D. Song, W. Gao, Y. C. Rong, L. J. Liu, L. Fang, and X. R. Xing, "Preparation and Electric Properties of $Bi_{0.5}Na_{0.5}TiO_3$-$Bi(Al_{0.5}\ Ga_{0.5})O_3$ Lead-Free Piezoceramics," *J. Am. Ceram. Soc.*, **96** [12] 3793–7 (2013).

[49]S. T. Zhang, F. Yan, and B. Yang, "Morphotropic Phase Boundary and Electrical Properties in $(1-x)Bi_{0.5}Na_{0.5}TiO_3$-$xBi(Zn_{0.5}Ti_{0.5})O_3$ Lead-Free Piezocera- Mics," *J. Appl. Phys.*, **107**, 114110, 4pp (2010).

[50]Q. Wang, J. Chen, L. L. Fan, L. J. Liu, L. Fang, and X. R. Xing, "Preparation and Electric Properties of $Bi_{0.5}Na_{0.5}TiO_3$-$Bi(Mg_{0.5}Ti_{0.5})O_3$ Lead-Free Piezoceramics," *J. Am. Ceram. Soc.*, **96** [4] 1171–5 (2013).

[51]W. F. Bai, Y. L. Bian, J. G. Hao, B. Shen, and J. W. Zhai, "The Composition and Temperature-Dependent Structure Evolution and Large Strain Response in $(1-x)(Bi_{0.5}Na_{0.5})TiO_3$-$xBa(Al_{0.5}Ta_{0.5})O_3$ Ceramics," *J. Am. Ceram. Soc.*, **96** [1] 246–52 (2013). □